ACADÉMIE
DES SCIENCES
INSTITUT DE FRANCE

Comptes Rendus

Géoscience

Sciences de la Planète

Jérôme Viers

A synthesis of copper isotope data for major continental and marine reservoirs

Volume 357 (2025), p. 299-313

Online since: 15 July 2025

https://doi.org/10.5802/crgeos.300

The Comptes Rendus. Géoscience — Sciences de la Planète *are a member of the Mersenne Center for open scientific publishing*
www.centre-mersenne.org — e-ISSN : 1778-7025

ACADÉMIE DES SCIENCES
INSTITUT DE FRANCE

Comptes Rendus. Géoscience — Sciences de la Planète
2025, Vol. 357, p. 299-313
https://doi.org/10.5802/crgeos.300

Review article
Critical zone and socio-ecosystems

A synthesis of copper isotope data for major continental and marine reservoirs

Jérôme Viers [a]

[a] Géosciences Environnement Toulouse (GET), Université de Toulouse, CNRS, IRD, 14 Avenue Edouard Belin, 31400, Toulouse, France
E-mail: jerome.viers@get.omp.eu

Abstract. The objective of this work is to make an inventory of copper isotope signatures (what amplitudes? what signs?) in the main reservoirs (rock, soil, river, oceans). After almost 25 years of work carried out with precise measurements of these isotopic ratios, it is important to consider whether they can provide us useful constraints in the understanding of the cycle of large-scale elements. The goal is not to discuss all the hypotheses of each paper, of each site, but to present the compilation of data in a neutral way and identify the significant features. This work should provide a simple, hard-hitting overview of the potential of this isotopic tool as a source tracer, but also of the main mechanisms at play within and between reservoirs.

Keywords. Copper isotopes, Signatures, Terrestrial and marine reservoirs.
Manuscript received 29 January 2025, revised 13 May 2025 and 19 June 2025, accepted 20 June 2025.

1. Introduction

Copper (Cu) is an essential element for the physiological functioning of living beings, but it can also be toxic in high concentrations (Flemming and Trevors, 1989; Brewer, 2010). It is also an indispensable metal for our societies, thanks to its many uses (transport, industry, communication, construction, agriculture). Demand for Cu is growing exponentially to meet the needs of both the world's growing population and the energy transition. Demand is such that even in Europe, where mining activity has been excessively low for the past thirty years, former mining areas such as Andalusia (Huelva region, Spain) are experiencing a significant mining revival (Buu-Sao, 2021).

Because of its economic importance, numerous works have been carried out to understand the development of Cu-rich mineralization (e.g., Mathur, Titley, et al., 2009) and thus facilitate mineral exploration. Given its massive use in all sectors of our societies, many studies have been carried out on the dispersion of copper in the continental and oceanic environments (e.g., Little, Vance, Walker-Brown, et al., 2014; Blotevogel, Schreck, et al., 2019). At the end of the 90s, the first precise measurements of the copper isotope ratio (i.e., $^{65}Cu/^{63}Cu$) were carried out by MC-ICP-MS (Maréchal et al., 1999), Cu having two stable isotopes (^{63}Cu and ^{65}Cu). The scientific community then began systematic measurements of this isotopic ratio in various environments (rocks, soils, rivers, sediments etc.) (Johnson et al., 2004; Teng et al., 2017; Moynier et al., 2017). The purpose of these studies was initially to make measurements in these reservoirs, and see if we could detect different isotope signatures. In a second step, the objective was to see if these signatures could be used as a source tracer or to understand the processes that induce them. In the latter case, understanding these processes opens a window of understanding on mechanisms that counteract the mobility of elements, in this case copper, in the natural environment (e.g., Borrok et al., 2008; Navarrete et al., 2011; Coutaud et al., 2018; Komárek et al., 2021).

The objective of this work is to make an inventory of copper isotope signatures (what amplitudes? what signs?) in the main reservoirs (rock, soil, river, oceans). After almost 25 years of work carried out with precise measurements of these isotopic ratios, it is important to consider whether they can provide us useful constraints in the understanding of the cycle of large-scale elements. The goal is not to discuss all the hypotheses of each paper, of each site, but to present the compilation of data in a neutral way and identify the significant features. This work should provide a simple, hard-hitting overview of the potential of this isotopic tool as a source tracer, but also of the main mechanisms at play within and between reservoirs. All the isotopic data presented are expressed in the form of δ^{65}Cu (in units of ‰) whose reference material is SRM-NIST 976:

$$\delta^{65}\mathrm{Cu}(‰) = \left(\left(\frac{\left(\frac{^{65}\mathrm{Cu}}{^{63}\mathrm{Cu}}\right)_{\mathrm{sample}}}{\left(\frac{^{65}\mathrm{Cu}}{^{63}\mathrm{Cu}}\right)_{\mathrm{NIST976}}} \right) - 1 \right) \times 1000. \qquad (1)$$

2. Rocks, mineralizations and alteration products (Figure 1)

Rocks (upper continental crust, mantle) show relatively low isotopic variability with the following mean values for δ^{65}Cu (‰): 0.02 ± 0.06 (granite), 0.41 ± 0.16 (granodiorite), −0.25 ± 0.44 (peridotite), 0.11 ± 0.08 (basalt), and 0.11 ± 0.16 for sedimentary rocks. These data are consistent with the value proposed by Savage et al. (2015) for the Bulk Silicate Earth (0.07 ± 0.1). The most striking result is the high isotopic variability of Cu-rich primary or secondary mineralization and associated reservoirs (ore, mining waste, precipitates, river sediments impacted by acid mine drainage). While primary sulfides (e.g., chalcopyrite) show an average value of 0.33 ± 1.66, variability is extreme for secondary products in natural or mining contexts ($-16.49 < \delta^{65}\mathrm{Cu}(‰) < 9.98$) (Mathur, Titley, et al., 2009) with an average value in the present data set of 0.07 ± 2.86. These secondary products may be either zones of secondary Cu enrichment (e.g. secondary chalcocite) (1.32 ± 1.26) or zones displaying the typical mineralogical assemblages of environments impacted by acid mine drainage with, in particular, ferrous minerals (e.g., goethite, hematite) or secondary sulfate minerals (e.g., jarosite, schwertmannite) (−1.59 ± 3.60). However, it seems that zones with secondary enrichment (chalcocite) are generally clearly positive, while leaching zones with a mixture of goethite, hematite and sulfates are negative (Mirnejad et al., 2010; Mathur, Ruiz, Casselman, et al., 2012; Mathur, Jin, et al., 2012). Experimental works (e.g., Ehrlich et al., 2004) have clearly shown that the dissolution of primary sulfide minerals results in the preferential departure of the heavy isotope (in the fluids), leaving an in-situ light-enriched solid residue. This result may seem contradictory to the synthesis of the data presented in Figure 1, where secondary products exhibit both positive or negative values. However, this high variability can be explained by the complexity of the water–rock interaction processes occurring in mineralized and/or mining areas. Indeed, in these environments, the dissolution of sulfides results in very charged percolating waters which can re-precipitate minerals, the latter may be dissolved under favorable conditions and so on (Lottermoser et al., 1999; Olias et al., 2006; Nieto et al., 2007). This succession of precipitation/dissolution may result in a high degree of fractionation (isotopic variability) in secondary products, solids and liquids, which can be both negative and positive (Perez Rodriguez et al., 2013). The strong isotopic amplitude in mining areas make copper isotopes a potentially relevant tracer for the study of metal transfer processes within these environments but also to assess the impact of these mining districts on continental and marine ecosystems.

3. Soils (Figure 2)

The first observation we can make is that soils exhibit a very low isotopic variability (−0.11 ± 0.19) and are generally enriched in the light isotope compared to the mean value of the rocks in the upper continental crust (see Section 2). However, we find that some soils may have much higher variability (S.-A. Liu, Teng, et al., 2014; Vance, Matthews, et al., 2016). The soil profile studied by S.-A. Liu, Teng, et al. (2014) in North Carolina (S6, Figure 2) reveals a high isotopic amplitude with values that can be high (0.4 ± 1) compared to the average soil. If we look at this study more closely, it appears that it is the surface soils which show strong joint enrichments of iron and copper that show these high isotopic values (up to 3.63).

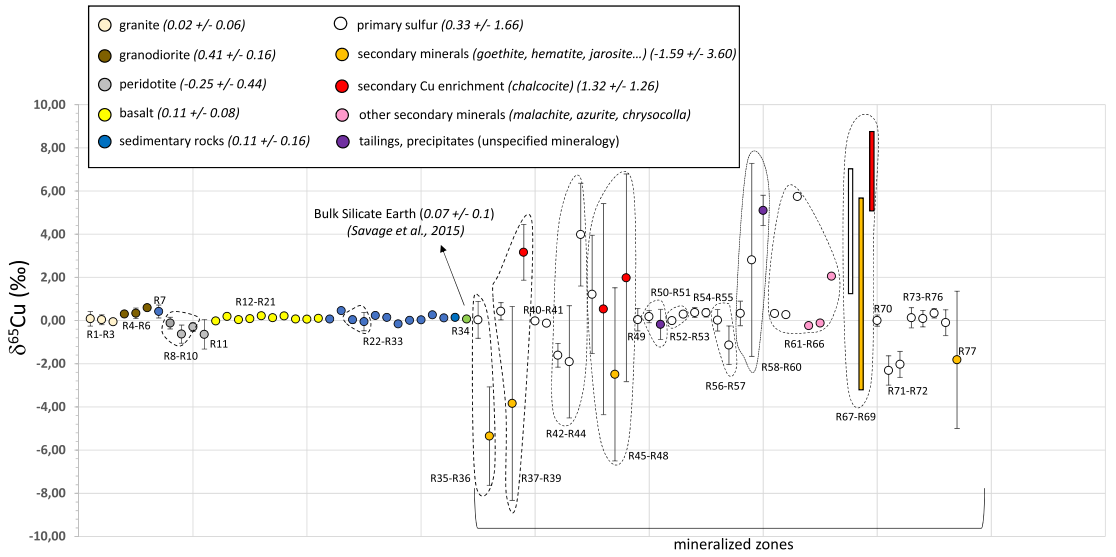

Figure 1. Type of sample and associated bibliographic reference for rocks, mineralization (ore) and alteration products; all data are presented in the form of δ^{65}Cu (in units of ‰) whose reference material is SRM-NIST976 (see Equation (1)). This is the case for all figures. For each reference, is reported a mean value associated with a standard deviation and the number of samples. Sometimes there is only one data. The points surrounded by a dotted line are from the same study and the reference (ex: S-6) allows to find the author and the associated values in the legend. R1: Granite from Lachlan Fold Belt (SE Australia) (0.08 ± 0.34 (n = 32); W. Li et al., 2009); R2: Granite from porphyry-type ore bodies (Lhasa, Tibet) (0.04 ± 0.23 (n = 4); Y.-C. Zheng et al., 2019); R3: Diorite from Central Asian Orogenic Belt (West China) (−0.06 (n = 1); Zhao et al., 2022); R4: Granodiorite (Colorado, USA) (= GSP-2, Certified Reference Material) (0.3 (n = 1); R.-R. Wang et al., 2022); R5: Granodiorite from porphyry-type ore bodies (Lhasa, Tibet) (0.34 ± 0.24 (n = 36); Y.-C. Zheng et al., 2019); R6: Granodiorite from Qulong porphyry copper deposit (Tibet) (0.59 ± 0.13 (n = 14); Nie et al., 2012); R7: Mafic enclave (Lhasa, Tibet) (0.42 ± 0.3 (n = 12); Y.-C. Zheng et al., 2019); R8: Lherzolite from Central Asian Orogenic Belt (West China) (−0.12 ± 0.27 (n = 11); Zhao et al., 2022); R9: Hornblende Lherzolite from Central Asian Orogenic Belt (West China) (−0.63 ± 0.42 (n = 6); Zhao et al., 2022); R10: Olivine Gabbro from Central Asian Orogenic Belt (West China) (−0.3 ± 0.2 (n = 8); Zhao et al., 2022); R11: Cratonic peridotite (China) (−0.64 ± 0.68 (n = 30); S.-A. Liu, Huang, et al., 2015); R12: Basalt (Iceland) (= BIR, Certified Reference Material) (−0.02 (n = 1); W. Li et al., 2009); R13: Columbia River Basalt (USA) (= BCR-1/2, Certified Reference Material) (0.19 (n = 1); K. V. Sullivan et al., 2022); R14: Diabase (Virginia, USA) (= W-2a Certified Reference Material) (0.04 (n = 1); K. Sullivan et al., 2020); R15: Hawaiian basalt (USA), (= BHVO-2, Certified Reference Material) (0.08 (n = 1); R.-R. Wang et al., 2022); R16: Basalt from Country Rock (Huangshannan, Huanshandong, Hulu and Tulaergen deposits, Eastern Tianshan, China) (0.22 ± 0.04 (n = 2); Zhao et al., 2022); R17: Basalt (Southwest Pacific Ocean, Niuatahi volcan, Tonga) (0.13 ± 0.10 (n = 3); Z. Wang et al., 2019); R18: Dacite (Southwest Pacific Ocean, Niuatahi volcan, Tonga) (0.21 ± 0.1 (n = 9); Z. Wang et al., 2019); R19: Basalt (Hainan Island, China) (0.07 (n = 1); J.-H. Liu et al., 2022); R20: Andesite (Oregon, USA), (= AGV-2, Certified Reference Material) (0.06 (n = 1); K. V. Sullivan et al., 2022); R21: Andesitic breccia tuff from Country Rock (Huangshannan, Huanshandong, Hulu and Tulaergen deposits, Eastern Tianshan, China) (0.10 ± 0.03 (n = 3); Zhao et al., 2022); R22: Cambrian micashist (southwest France) (0.07 (n = 1); El Azzi et al., 2013); R23: Biotite quartz schist from Country Rock (Huangshannan, Huanshandong, Hulu and Tulaergen deposits, Eastern Tianshan, China) (0.46 ± 0.04 (n = 2); Zhao et al., 2022); R24: Shale (Marcellus formation, USA) (0.04 ± 0.16 (n = 8); Mathur, Jin, et al., 2012); R25: Black shales (South Africa) (−0.05 ± 0.42 (n = 11); Chi-Fru et al., 2016);

Figure 1. (**cont.**) R26: Black shales (Gabon) (0.23 ± 0.09 (n = 8); Chi-Fru et al., 2016); R27: Black shales (Maokou formation, China) (0.14 ± 0.09 (n = 5); Lv et al., 2016); R28: Cody Shale (USA) (= SCo-1, Certified Reference Material) (−0.16 (n = 1); Sossi et al., 2014); R29: Loess (China) (0.01 ± 0.03 (n = 2); W. Li et al., 2009); R30: Greywacke (Goa state, India) (0.03 (n = 1); Little, Munson, et al., 2019); R31: Sandstone (0.26 ± 0.12 (n = 2); Zhao et al., 2022); R32: Bedrock (Fluvio-lacustrine sediments) (China) (0.12 ± 0.01 (n = 2); Ren et al., 2022); R33: Tuffite (Slovakia) (0.14 (n = 1); Bigalke, Weyer, Kobza, et al., 2010); R34: Bulk Silicate Earth (MORB + OIB + Komatite + Peridotite) (0.07 ± 0.1; Savage et al., 2015); R35: Mix of chalcopyrite, chalcocite, djurleite, and covellite from Canariaco district (Peru) (0.03 ± 0.85 (n = 37); Mathur, Ruiz, Casselman, et al., 2012); R36: Mix of goethite and hematite from Canariaco district (Peru) (−5.35 ± 2.28 (n = 7); Mathur, Ruiz, Casselman, et al., 2012); R37: Mix of chalcopyrite and pyrite from Urumieh-Dokhtar magmatic belt (Iran) (0.43 ± 0.4 (n = 10); Mirnejad et al., 2010); R38: Mix of hematite and goethite from Urumieh-Dokhtar magmatic belt (Iran) (−3.84 ± 4.49 (n = 10); Mirnejad et al., 2010); R39: Supergene chalcocite from Urumieh-Dokhtar magmatic belt (Iran) (3.16 ± 1.29 (n = 11); Mirnejad et al., 2010); R40: Cu–Co ore (= SU-1, Certified Reference Material) (−0.02; Chapman et al., 2005); R41: Mix of Pyrite, chalcopyrite, galene, and sericite from Prospect Gulch abandoned mine (Colorado, USA) (−0.13 ± 0.1 (n = 2); Fernandez and Borrok, 2009); R42: Chalcopyrite ore (skarn type) (China) (−1.61 ± 0.55 (n = 3); Mathur, Munk, et al., 2014); R43: Chalcopyrite and pyrite (massive sulfide, Spain) (−1.91 ± 2.6 (n = 15); Mathur, Munk, et al., 2014); R44: Chalcopyrite and pyrite (porphyry copper deposit, Chile) (3.98 ± 2.38 (n = 4); Mathur, Munk, et al., 2014); R45: Chalcopyrite and pyrite from 9 porphyry copper deposits (USA, Chile, Turkey) (1.21 ± 2.74 (n = 7); Mathur, Titley, et al., 2009); R46: Secondary chalcocite (0.53 ± 4.89 (n = 15); Mathur, Titley, et al., 2009); R47: Leach cap (mix of hematite, jarosite and goethite) (−2.49 ± 4.01 (n = 5); Mathur, Titley, et al., 2009); R48: Oxide (1.98 ± 4.81 (n = 10); Mathur, Titley, et al., 2009); R49: Chalcopyrite (USA, Peru) (0.04 ± 0.52 (n = 38); Larson et al., 2003); R50: Pyrite from Mining district of Taxco (southern Mexico) (0.18 ± 0.28 (n = 4); Dótor-Almazán et al., 2017); R51: Tailings and precipitates from mining district of Taxco (southern Mexico) (−0.18 ± 0.70 (n = 14); Dótor-Almazán et al., 2017); R52: Chalcopyrite (Colorado, USA) (−0.01 (n = 1); Kimball et al., 2009); R53: Enargite (Colorado, USA) (0.29 (n = 1); Kimball et al., 2009); R54: Chalcopyrite (0.37 ± 0.23 (n = 29); Y.-C. Zheng et al., 2019); R55: Chalcopyrite (0.36 ± 0.2; Z. Q. Li et al., 2009); R56: Chalcopyrite (Schwarzwald area, South Germany) (0.014 ± 0.5 (n = 25); Markl et al., 2006); R57: Oxidized chalcopyrite (Schwarzwald area, south Germany) (−1.14 ± 0.89 (n = 3); Markl et al., 2006); R58: Chalcopyrite (Dexing mine, China) (0.33 ± 0.57 (n = 9); Song et al., 2016); R59: Pyrite from Dexing mine (China) (2.81 ± 4.47 (n = 15); Song et al., 2016); R60: Tailings from Dexing mine (China) (5.1 ± 0.7 (n = 4); Song et al., 2016); R61: Chalcopyrite (Lau Basin, Pacific) (0.32 (n = 1); Maréchal et al., 1999); R62: Chalcopyrite (Chuquicamata, Péru) (0.27 (n = 1); Maréchal et al., 1999); R63: Chalcopyrite (Morenci, USA) (5.74 (n = 1); Maréchal et al., 1999); R64: Malachite (Zaire) (−0.24 (n = 1); Maréchal et al., 1999); R65: Chrysocolla (Bagdad, USA) (−0.12 (n = 1); Maréchal et al., 1999); R66: Azurite (Chessy, France) (2.05 (n = 1); Maréchal et al., 1999); R67: Hypogene zone from Kerman Porphyry Copper Belt (Iran) (1.49–7.31 (range); Sarjoughian et al., 2024); R68: Leached zone from Kerman Porphyry Copper Belt (Iran) (−3.41 to 5.82 (range); Sarjoughian et al., 2024); R69: Supergene enriched zone with secondary minerals (Kerman Porphyry Copper Belt, Iran) (5.18–8.71 (range); Sarjoughian et al., 2024); R70: Chalcopyrite (Cu–Pb–Zn deposit from Mount Isa, Australia) (−0 ± 0.26 (n = 12); Mahan et al., 2023); R71: Cu sulphide minerals within porphyries (−2.31 ± 0.68 (n = 9); Asael et al., 2007); R72: Cu sulphide minerals within Cambrian dolomite (−2.03 ± 0.6 (n = 13); Asael et al., 2007); R73: Chalcopyrite (0.13 ± 0.47 (n = 3); Kim et al., 2023); R74: Chalcopyrite (Chile) (0.09 ± 0.38 (n = 24); Mathur, Ruiz, Titley, et al., 2005); R75: Chalcopyrite from the skarn ore bodies (Hongshan-Hongniu deposit, China) (0.34 ± 0.22 (n = 28); P. Wang et al., 2017); R76: Chalcopyrite from Dabu porphyry Cu–Mo deposit (Tibet) (−0.10 ± 0.60 (n = 22); S. Wu et al., 2017); R77: Secondary minerals from bed rivers and open pits impacted by Tharsis Mine (Huelva, Spain) (−1.82 ± 3.18 (n = 9); Viers, Freydier, et al., 2023).

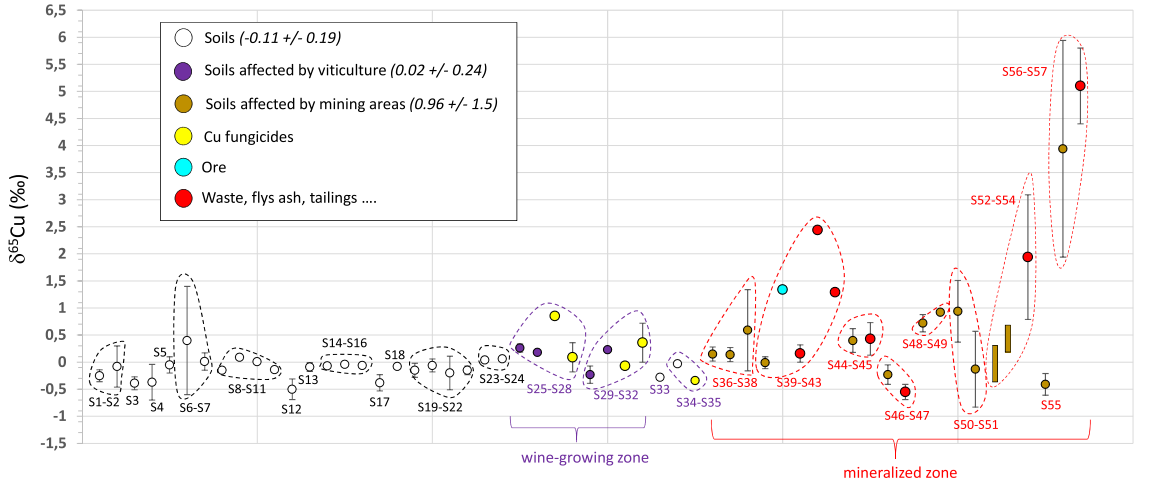

Figure 2. Type of sample and associated bibliographic reference for soils; The points surrounded by a dotted line are from the same study. S1: Fluvisol (Glen Feshie chronosequence, Scotland, United Kingdom) (−0.25 ± 0.11 (n = 20); Vance, Matthews, et al., 2016); S2: Andisol from Hawaii (USA) (−0.08 ± 0.38 (n = 54); Vance, Matthews, et al., 2016); S3: Lateritic soils from Amazonia (Brazil) (−0.39 ± 0.12 (n = 8); Guinoiseau et al., 2017); S4: Lateritic soils from Goa state (India) (−0.37 ± 0.33 (n = 14); Little, Munson, et al., 2019); S5: Lateritic soils from Penglai weathering profile (Hainan Island, China) (−0.05 ± 0.15 (n = 19); J.-H. Liu et al., 2022); S6: Saprolitic soils on basalt (South Carolina, USA) (0.4 ± 1 (n = 17); S.-A. Liu, Teng, et al., 2014); S7: Soils on basalt from Hainan Island (China) (0.01 ± 0.16 (n = 19); S.-A. Liu, Teng, et al., 2014); S8: Arenosol from the French Soil Quality Monitoring (France) (−0.15 (n = 1); Fekiacova et al., 2015); S9: Cambisol (on basalt) from the French Soil Quality Monitoring (France) (0.09 (n = 1); Fekiacova et al., 2015); S10: Cambisol (on granit) from the French Soil Quality Monitoring (France) (0.01 (n = 1); Fekiacova et al., 2015); S11: Podzol from the French Soil Quality Monitoring (France) (−0.14 (n = 1); Fekiacova et al., 2015); S12: Soils on Marcellus formation (Pennsylvania, USA) (−0.5 ± 0.19 (n = 33); Mathur, Jin, et al., 2012); S13: Paddy soil, gley horizon (Suzhou, Eastern China) (−0.09 ± 0.08 (n = 33); R.-R. Wang et al., 2022); S14: Liaohe plain Soil (= GBW07425 (GSS-11, Certified Reference Material) (−0.07 (n = 1); K. V. Sullivan et al., 2022); S15: Paddy soil (GBW07443) (GSF-3, Certified Reference Material) (−0.04 (n = 1); K. V. Sullivan et al., 2022); S16: Soil from North China Plain (GBW07389) (GSS-33, Certified Reference Material) (−0.06 (n = 1); K. V. Sullivan et al., 2022); S17: Deeper horizon from retisol (Yonne Plateau, France) (−0.38 ± 0.15 (n = 19); Kusonwiriyawong, Bigalke, Cornu, et al., 2017); S18: Carbonatic alluvial soil (floodplain, Switzerland) (−0.08; Kusonwiriyawong, Bigalke, Abgottspon, et al., 2016); S19: Skeletic cambisol developed on slate (Germany) (−0.15 ± 0.13 (n = 4); Bigalke, Weyer and Wilcke, 2011); S20: Dystric cambisol on sandstone (Slovakia) (−0.06 ± 0.12 (n = 7); Bigalke, Weyer and Wilcke, 2011); S21: Haplic podzol (Germany) (−0.20 ± 0.31 (n = 10); Bigalke, Weyer and Wilcke, 2011); S22: Haplic podzol (Slovakia) (−0.15 ± 0.08 (n = 6); Bigalke, Weyer and Wilcke, 2011); S23: Cultivated paddy soils (Mun River Basin, Thailand) (0.04; X. Zheng et al., 2023); S24: Abandoned paddy soils (Mun River Basin, Thailand) (0.06 (n = 1); X. Zheng et al., 2023); S25: Vertic cambisol (Vineyard catchment, Italia) (0.26 ± 0.08 (n = 8); Blotevogel, Oliva, et al., 2018); S26: Calcaric cambisol (Vineyard catchment, Italia) (0.18 ± 0.03 (n = 7); Blotevogel, Oliva, et al., 2018); S27: Fungicides (Cu sulfates) (0.85 ± 0.05 (n = 2); Blotevogel, Oliva, et al., 2018); S28: Fungicides (Cu hydroxydes) (0.09 ± 0.27 (n = 8); Blotevogel, Oliva, et al., 2018); S29: Fine clays fraction from Cambisol (Vineyard catchment) (−0.23 ± 0.16 (n = 8); Babcsanyi et al., 2016); S30: Silt fraction from Cambisol (Vineyard catchment) (0.23 ± 0.04 (n = 4); Babcsanyi et al., 2016); S31: Fungicides (Cu sulfates) (−0.07 ± 0.01 (n = 2); Babcsanyi et al., 2016); S32: Fungicides (Cu hydroxydes) (0.36 ± 0.36 (n = 4); Babcsanyi et al., 2016);

Figure 2. (**cont.**) S33: Soils from Bordeaux (Vineyard catchment, France) (−0.28 ± 0.03 (n = 3); Petit, Schäfer, et al., 2013); S34: Soils from Banyuls (Vineyard catchment, France) (−0.03 ± 0.03 (n = 2); El Azzi et al., 2013); S35: Cu fungicides (−0.34 (n = 1); El Azzi et al., 2013); S36: Dystric Cambisol (1 km–3.8 km from smelter, Slovakia) (0.15 ± 0.13 (n = 12); Bigalke, Weyer, Kobza, et al., 2010); S37: Stagni eutric cambisol (0.14 ± 0.13 (n = 6); Bigalke, Weyer, Kobza, et al., 2010); S38: Waste products (slag, ash, solid waste) (Slovakia) (0.59 ± 0.75 (n = 5); Bigalke, Weyer, Kobza, et al., 2010); S39: Top soils from Panhihua city area (Sichuan province, China) (−0.01 ± 0.11 (n = 19); Xia et al., 2023); S40: Ore from Panhihua city area (Sichuan province, China) (1.34 (n = 1); Xia et al., 2023); S41: Fly ash from Panhihua city area (Sichuan province, China) (0.16 ± 0.16 (n = 3); Xia et al., 2023); S42: Coal from Panhihua city area (Sichuan province, China) (2.44 (n = 1); Xia et al., 2023); S43: Smelting slag from Panhihua city area (Sichuan province, China) (1.29 (n = 1); Xia et al., 2023); S44: Contaminated soils (Tsumeb district, Namibia) (0.4 ± 0.22 (n = 8); Kribek et al., 2018); S45: Slag flotation tailings, smelter dust … (Tsumeb district, Namibia) (0.43 ± 0.3 (n = 18); Kribek et al., 2018); S46: Polluted soils from Copperbelt (Zambia) (−0.23 ± 0.18 (n = 13); Mihaljevic et al., 2018); S47: Concentrates processed in the smelter (Zambia) (−0.55 ± 0.14 (n = 4); Mihaljevic et al., 2018); S48: Contaminated soils from coal mining area (Suixi County, soutwest Huaibei city, China) (0.72 ± 0.16 (n = 17); Ren et al., 2022); S49: Flying ash coal mining area (Suixi County, soutwest Huaibei city, China) (0.92 (n = 1); Ren et al., 2022); S50: Soils from mining region of Taxco area (southern Mexico) (0.94 ± 0.57 (n = 5); Dótor-Almazán et al., 2017); S51: Tailing and precipitates from mining region of Taxco area (southern Mexico) (−0.13 ± 0.7 (n = 15); Dótor-Almazán et al., 2017); S52: Soil close to abandoned Dalseong Cu–W mine (Republic of Korea) (−0.46 to 0.32 (range); Kim et al., 2023); S53: Soil downstream the adit seepage (abandoned Dalseong Cu–W mine, Republic of Korea) (0.41–1.12 (range); Kim et al., 2023); S54: Adit seepages from Dalseong Cu–W mine (Republic of Korea) (1.94± 1.15 (n = 9); Kim et al., 2023); S55: Soils (colluviosol or leptosol) on limestone Marseille (−0.41 ± 0.2 (n = 9); Gelly et al., 2019); S56: Soil from Dexing mine (China) (3.94 ± 2 (n = 2); Song et al., 2016); S57: Tailings from Dexing mine (China) (5.1 ± 0.7 (n = 4); Song et al., 2016).

These data agree with the work of Balistrieri et al. (2008) and Pokrovsky et al. (2008) showing that the sorption of Cu onto amorphous Fe(III) metallic oxyhydroxides favors the heavy isotope. Note also that some soils (Andisol) in Hawaii may have high signatures which are explained by an input of Asian dust that contributes significantly to the Cu budget (Vance, Matthews, et al., 2016). However, in general, the global isotopic value we obtained for soils suggests that the pedogenetic processes induce the preferential leaching of the heavy isotope (^{65}Cu). This signifies that the products (dissolved and particulate matter) of these weathering processes exported out of the soil should therefore exhibit an isotopic signature higher than that of soils. In other words, this suggests that the material transported by rivers must have a heavier overall signature than "average" soils.

Soils impacted by strong anthropogenic activities also show differences in isotopic composition compared to the average soil. Among soils impacted by winegrowing, it appears that they can present a negative signature (e.g., Bordeaux region, France, −0.37 to −0.28; S33, Figure 2; Petit, Schäfer, et al., 2013) or positive (e.g., Soave region, Italy; 0.18–0.26; S25–S26, Figure 2; Blotevogel, Oliva, et al., 2018). This contrast can be explained by the high isotopic variability of copper brought into vineyards as a fungicide ($-0.34 < \delta^{65}\mathrm{Cu}(‰) < 0.85$; 0.3 ± 0.4). We obtained an average value of 0.02 ± 0.24 for soils impacted by winegrowing. Another particularity concerns soils impacted by mining activities and/or processing (in particular pyrometallurgy) which generally show a significantly heavier signature than average soils (0.96 ± 1.5). However, if this general trend is emerging, it should not obscure the fact that differences can be found locally, at certain sites. This can be illustrated by the work of Mihaljevic et al. (2018). Indeed, on this site of Zambia impacted by mining activity, the soils are isotopically negative (−0.43 ± 0.06‰) as are the mine tailings (−0.75 to −0.45‰; Mihaljevic et al., 2018). These soils impacted by viticulture or mining activities do not seem to follow a general rule regarding the sign and amplitude of fractionation.

It is therefore important to properly characterize their reservoirs/sources and their isotopic signatures at a local scale. However, the magnitude of these fractionations makes the use of copper isotopes relevant in such contexts. Their use in natural contexts for the study of pedogenetic processes seems more limited.

4. World rivers (Figure 3)

In Figure 3, are plotted river data for dissolved phase (<0.22 μm or 0.45 μm), suspended sediment (>0.22 μm or 0.45 μm) and bottom sediments. If we consider unpolluted rivers, that is to say "just" subject to global diffuse pollution, it emerges that the dissolved phase of rivers shows relatively high isotopic variability (between $-0.25 < \delta^{65}Cu_{Dissolved}$ (‰) < 1.68). In 2008, Vance et al. proposed a global average value for the dissolved fraction of rivers of 0.68‰. Vance, Archer, et al. (2008) suggest that the high value for the dissolved phase of rivers is related to the preferential complexation of heavy copper with organic ligands, as shown by the work of Ryan et al. (2014) and Bigalke, Weyer and Wilcke (2010). Compared to this average value proposed by Vance, Archer, et al. (2008), it appears that some rivers may have much more negative values [−0.25‰ (Khamchanka, Russia); R27, Figure 3; Viers (unp. value)] or much more positive ones (1.18 ± 0.3‰ for Yangtze River, China; R35, Figure 3; Q. Wang et al., 2020). Q. Wang et al. (ibid.) recognized that the values obtained for the Yangtze River and its tributaries are the highest ever measured; moreover, unpublished measurement (Viers) confirm these high values for the Yangtze River (R22, Figure 3). Q. Wang et al. (ibid.) attribute these high values to the effect of the Three Gorges Dam; the accumulation of sediment within the dam would favor the preferential sorption of the light isotope onto mineral surface leaving a heavier copper in the dissolved phase complexed with organic matter. Even if another average value is proposed in this paper (0.53 ± 0.45) for the dissolved phase of world rivers, to my opinion, proposing a rigorous weighted average flow value requires a broader sampling of other major rivers (e.g., Orinoco, Mekong, Congo, Yenisey, Lena) which provide a significant contribution of the Cu budget to the world ocean and for which we don't have any data. It also seems necessary to see whether the isotopic signature in copper for these large river systems varies during the seasons, that is to say the hydrological year. There is, however, another aspect to be considered here. Some studies suggest that the flow of Cu to the World Ocean via rivers could be largely underestimated and in particular the transfer of Cu through coastal mining areas (Olias et al., 2006). This is the case, for example, of the Iberian Pyritic Belt (Huelva region, Spain) where the Tinto and Odiel rivers would export to the Atlantic Ocean almost 10% of the world's copper flow (ibid.) due to the presence of nearly 90 abandoned mines in the watersheds of these rivers. We understand that given the particular signature of these rivers (−0.74 ± 0.27 and −0.45 ± 0.66 for Odiel and Tinto rivers, respectively; R52 and R53, Figure 3; Borrok et al., 2008), this region (and similar coastal regions) may influence the global isotopic signature of the world's ocean. It is important to note that the rivers draining areas impacted by mining activities are those with the highest isotopic amplitude (0.28 ± 1.84). Given what we observed for solids (precipitates, sediments, ore) in these mining areas, it is not surprising to find this high amplitude for watercourses.

It also emerges from this synthesis that sediments show more negative signatures than the dissolved phase of rivers ($-0.55 < \delta^{65}Cu_{Sediment}$ (‰) < 0.23) with an average value of −0.09 ± 0.20. If we consider, based on literature data (e.g., Boyle et al., 1977; Viers, Dupré, et al., 2009; Little, Vance, Walker-Brown, et al., 2014; Gaillardet et al., 2014; Takano, Tanimizu, et al., 2014; L. Li et al., 2020; Machu et al., 2024) that 90% of the copper is exported in particulates, a simple mixing calculation reveals that rivers export to the world ocean a whole copper close to 0 or slightly negative depending on whether one considers the value proposed by Vance, Archer, et al. (2008) or that of this article. Considering such a distribution, this isotopic signature of this whole material transported by rivers seems contradictory because it was thought to find the missing fraction of the soils and therefore a rather positive pool was expected. This apparent bias may be linked to a still too incomplete database that does not properly represent the reality of the isotopic signatures of these reservoirs (soils, river sediments) or the isotopic signatures observed in watercourses are impacted by secondary exchange/redistribution processes fractionating copper isotopes within watercourses.

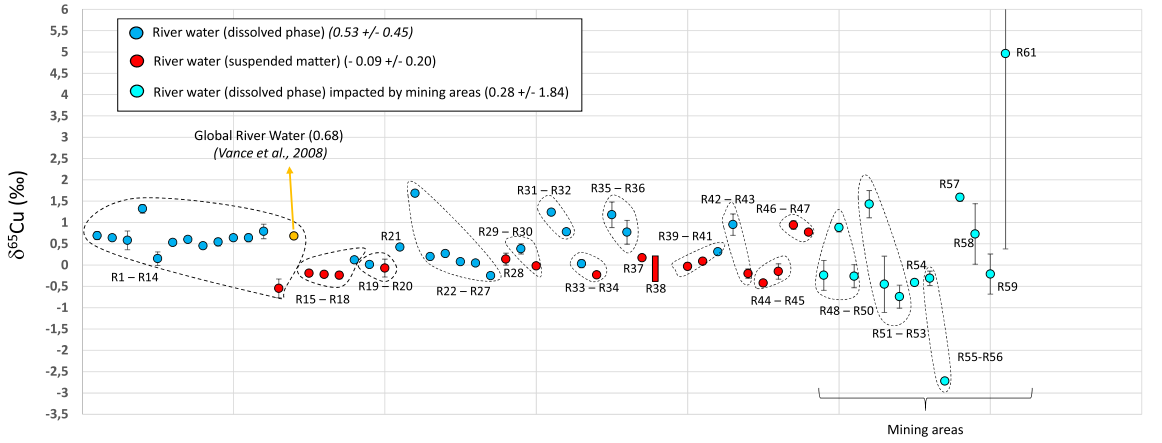

Figure 3. Type of sample and associated bibliographic reference for river waters. R1: Amazon River (Brazil) (0.69 ± 0.09 (n = 3); Vance, Archer, et al., 2008); R2: Brahmaputra River (India) (0.64 (n = 1); Vance, Archer, et al., 2008); R3: Nile River (Sudan, Egypt) (0.58 ± 0.22 (n = 18); Vance, Archer, et al., 2008); R4: Chang-Jiang (Yangtze) River (China) (1.32 ± 0.1 (n = 13); Vance, Archer, et al., 2008); R5: Missouri River (USA) (0.15 ± 0.16 (n = 4); Vance, Archer, et al., 2008); R6: Kalix River (Sweden) (0.53 ± 0.07 (n = 7); Vance, Archer, et al., 2008); R7: River from Kamtchanka (Russia) (0.6 (n = 1); Vance, Archer, et al., 2008); R8: Ottawa River (Canada) (0.45 ± 0.06 (n = 2); Vance, Archer, et al., 2008); R9: Tocantins River (Brazil) (0.54 ± 0.09 (n = 3); Vance, Archer, et al., 2008); R10: Volga River (Russia) (0.64 ± 0.01 (n = 2); Vance, Archer, et al., 2008); R11: Itchen River (England) (0.64 ± 0.09 (n = 19); Vance, Archer, et al., 2008); R12: Beaulieu River (England) (0.79 ± 0.17 (n = 7); Vance, Archer, et al., 2008); R13: Suspended matter from Itchen River (England) (−0.55 ± 0.22 (n = 16); Vance, Archer, et al., 2008); R14: Global River Water (0.68; Vance, Archer, et al., 2008); R15: Suspended matter from Lot River (France) (−0.19 (n = 1); Petit, Schäfer, et al., 2013); R16: Suspended matter from Gironde (France) (−0.22 (n = 1); Petit, Schäfer, et al., 2013); R17: Suspended matter from Garonne River (France) (−0.24 ± 0.08 (n = 13); Petit, Schäfer, et al., 2013); R18: Garonne River (France) (0.12 (n = 1); Petit, Schäfer, et al., 2013); R19: Scheldt Estuary (Belgium) (0.01 (n = 1); Petit, de Jong, et al., 2008); R20: Bed sediment from Scheldt Estuary (Belgium) (−0.07 ± 0.21 (n = 7); Petit, de Jong, et al., 2008); R21: Palojoki River (Karely, Russia) (0.42 ± 0.05 (n = 3); Ilina et al., 2013); R22: Yangtze River (China) [1.68 (n = 1); Viers, unpublished data]; R23: River from China [0.20 (n = 1); Viers, unpublished data]; R24: River from Canada [0.27 (n = 1); Viers, unpublished data]; R25: river from Siberia (Russia) [0.08 (n = 1); Viers, unpublished data]; R26: River from Siberia (Russia) [0.05 (n = 1); Viers, unpublished data]; R27: Rivers from Khamtchanka Peninsula (Russia) [−0.25 ± 0.06 (n = 5); Viers, unpublished data]; R28: Suspended matter from Negro River (Brazil) (0.14 ± 0.14 (n = 16); Guinoiseau et al., 2017); R29: St Lawrence River (Canada) (0.38 (n = 1); K. V. Sullivan et al., 2022); R30: Floodplain sediment (China) (−0.02 (n = 1); K. V. Sullivan et al., 2022); R31: Tawara River (Japan) (1.24 ± 0.05 (n = 6); Takano, Tsuchiya, et al., 2021); R32: Uji River (Japan) (0.78; Takano, Tsuchiya, et al., 2021); R33: Glen Feshie River (Scotland) (0.03 ± 0.09 (n = 5); Vance, Matthews, et al., 2016); R34: Alluvium from Glen Feshie River (Scotland) (−0.23 (n = 1); Vance, Matthews, et al., 2016); R35: Chang-Jiang (Yangtze) River (China) (1.18 ± 0.3 (n = 20); Q. Wang et al., 2020); R36: Tributaries of the Yangtze River (China) (0.77 ± 0.28 (n = 7); Q. Wang et al., 2020); R37: Suspended matter from Zhujiang River (China) (0.17 ± 0.02 (n = 22); Zeng and Han, 2020); R38: Bed sediments from Huangpu River (tributary of the Yangtze river, China) (−0.37 to 0.18 (range); Tu et al., 2023); R39: Bed sediment from Baillaury River (Banyuls, France) (−0.03 ± 0.08 (n = 3); El Azzi et al., 2013); R40: Suspended matter from Baillaury River (Banyuls, France) (0.09 (n = 1); El Azzi et al., 2013); R41: Baillaury River (Banyuls, France) (0.31 (n = 1); El Azzi et al., 2013); R42: River from vineyard catchment (Alsace, France) (0.95 ± 0.25 (n = 9); Babcsanyi et al., 2016); R43: Suspended matter from vineyard catchment (Alsace, France) (−0.20 ± 0.11 (n = 9); Babcsanyi et al., 2016);

Figure 3. (**cont**.) R44: Sediment from urbanized area (Guanabara bay, Rio de Janeiro, Brazil) (−0.42 ± 0.05 (n = 5); Barreira et al., 2024); R45: Sediment from slightly urbanized area (Guanabara bay, Rio de Janeiro, Brazil) (−0.15 ± 0.18 (n = 5); Barreira et al., 2024); R46: Smelter impacted sediment from Ballinger lake (USA) (0.94 ± 0.1 (n = 11); Thapalia et al., 2010); R47: Sediment from Ballinger lake (USA) (0.77 ± 0.06 (n = x); Thapalia et al., 2010); R48: Spanish River (Great Lakes region, Canada) (−0.24 ± 0.35 (n = 8); Junqueira et al., 2023); R49: Mine waste seepage (Spanish River, Great Lakes region, Canada) (0.88 ± 0.1 (n = 2); Junqueira et al., 2023); R50: Trent River (Great Lakes region, Canada) (−0.26 ± 0.27 (n = 8); Junqueira et al., 2023); R51: Fischer Creek (USA) (1.43 ± 0.32 (n = 13); Borrok et al., 2008); R52: Tinto River (Iberian Pyrite Belt, Spain) (−0.45 ± 0.66 (n = 5); Borrok et al., 2008); R53: Odiel River (Iberian Pyrite Belt, Spain) (−0.74 ± 0.27 (n = 5); Borrok et al., 2008); R54: West Branch Ompampanoosuc River (−0.41 (n = 1); Balistrieri et al., 2008); R55: Meca River (Odiel River tributary, Iberian Pyrite Belt, Spain) (−0.31 ± 0.17 (n = 17); Masbou et al., 2020); R56: Meca River tributary (Iberian Pyrite Belt, Spain) (−2.72 (n = 1); Masbou et al., 2020); R57: Rivers from mining region of Colorado (USA) (1.59 ± 0.09 (n = 14); Kimball et al., 2009); R58: Cobica River (Iberian Pyrite Belt, Spain) (0.73 ± 0.71 (n = 4); Viers, J. A. Grande, et al., 2018); R59: Meca River (Odiel River tributary, Iberian Pyrite Belt, Spain) (−0.21 ± 0.47 (n = 7); Viers, Freydier, et al., 2023); R60: Rivers from Dexing mine region (China) (4.96 ± 4.58 (n = 20); Song et al., 2016).

5. Oceans (Figure 4)

Given the limited data available, it appears that the World Ocean has an average value of 0.63 ± 0.12‰ in agreement with literature data (Little, Archer, et al., 2018). This isotopic signature of the oceans ranges from 0.50‰ (Mediterranean Sea and Atlantic Ocean) to 0.85‰ (North Pacific Ocean). The most striking result, however, is the difference in isotopic composition between the dissolved phase (0.63 ± 0.12‰) and the particulate phase (0.07 ± 0.17‰), enriched in the light isotope. We find here a similarity with the dissolved and particulate phases of rivers, for which we have also an isotopically dissolved phase heavier than the particulate phase. A number of articles (e.g., Vance, Archer, et al., 2008; Takano, Tanimizu, et al., 2014; Little, Vance, Walker-Brown, et al., 2014; Sherman and Little, 2020) have attempted to explain the copper cycle within the oceans and the associated isotopic fractionations during intra-oceanic processes (inputs from rivers and the atmosphere, intra-oceanic exchange between dissolved and particulate matter, role of planktonic matter and Fe–Mn nodules). In particular, these authors (e.g., Little, Archer, et al., 2018) point out that if the signature of the ocean is similar (0.65‰) to that provided by rivers (0.68‰) a mass balance in stationary state requires an additional source of light Cu. This source of light Cu could be hydrothermalism or the dissolution of terrigenous particles, brought by rivers or the atmosphere. However, the establishment of these balance sheets is subject to high uncertainties regarding flows and associated isotopic signatures. While the signature of the particles brought by the rivers seems homogeneous and well constrained, it is not the same for the dissolved phase. There is also considerable uncertainty about the isotopic signature of atmospheric particles. If it seems that particles in cities have isotopic signatures between 0 and 0.6 (global diffuse pollution of urban environments; Souto-Oliveira et al., 2018; Dong, Ochoa Gonzalez, et al., 2017; Ochoa Gonzalez et al., 2016), the few measurements available for non-anthropized environments (Sahel Region (Africa), Taklamakan desert (Asia), equatorial eastern North Atlantic region of West Africa, eastern tropical Atlantic; South China Sea) reveal values in a more negative range (−0.24 to 0.83) (Dong, Weiss, et al., 2013; Packman et al., 2022; Takano, Liao, Tian, et al., 2020). Aerosols values obtained for sites heavily impacted by mineral processing activities in Central Europe appear very negative (−3.63 to 0.42) (Novak et al., 2016; Mihaljevic et al., 2018). Another striking fact resulting from this synthesis is that there is no major isotopic difference between the signature of marine particles and those of harbor sediments impacted by anthropogenic activities (Briant et al., 2022; Jeong, Araujo, Garnier, et al., 2023; Jeong, Araujo, Knoery, et al., 2023). These data appear similar to the mean value for terrestrial rocks.

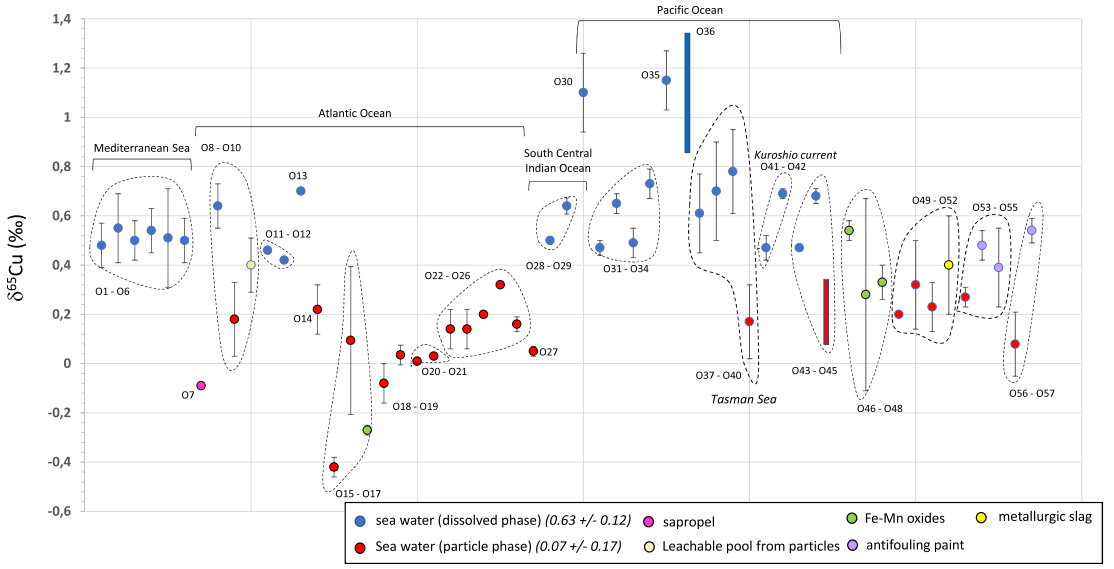

Figure 4. Type of sample and associated bibliographic reference for Oceans; the points surrounded by a dotted line proviennent d'une même zone géographique (China sea, Pacific Ocean). O1: Mediterranean sea (0.51 ± 0.2 (n = 96); Baconnais et al., 2019); O2: South Western Mediterranean sea (0.48 ± 0.09 (n = 23); Baconnais et al., 2019); O3: South Eastern Mediterranean sea (0.55 ± 0.14 (n = 19); Baconnais et al., 2019); O4: North Western Mediterranean sea (0.50 ± 0.08 (n = 21); Baconnais et al., 2019); O5: North Eastern Mediterranean sea (0.54 ± 0.09 (n = 14); Baconnais et al., 2019); O6: North Atlantic Ocean (0.50 ± 0.09 (n = 20); Baconnais et al., 2019); O7: Sapropel (−0.09 (n = 1); Maréchal et al., 1999); O8: South Atlantic (0.64 ± 0.09 (n = 63); Little, Archer, et al., 2018); O9: Particles from South Atlantic (0.18 ± 0.15 (n = 17); Little, Archer, et al., 2018); O10: Leachable pool from particles from South Atlantic (0.4 ± 0.11 (n = 16); Little, Archer, et al., 2018); O11: Near shore seawater (Halifax Harbour, North Atlantic) (= CASS-5 reference material) (0.46; K. V. Sullivan et al., 2022); O12: Seawater (Nova Scotia, North Atlantic) (NASS-6 reference material) (0.42; K. V. Sullivan et al., 2022); O13: English channel (0.7 (n = 1); Bermin et al., 2006); O14: Sediment from Atlantic Ocean (0.22 ± 0.1 (n = 8); Maréchal et al., 1999); O15: Suspended particle (lower fraction, <250 µm) from continental shelf of northern Bay of Biscay (north eastern Atlantic Ocean) (−0.42 ± 0.04 (n = 2); Araujo, Knoery, et al., 2022); O16: Suspended particle (coarse fraction, >250 µm) from inner continental shelf of northern Bay of Biscay (north eastern Atlantic Ocean) (0.09 ± 0.03 (n = 5); Araujo, Knoery, et al., 2022); O17: Plankton, BCR 414 Certified Reference Material) (−0.27 (n = 1); Araujo, Knoery, et al., 2022); O18: Surface sediments from the Loire estuary (France) (−0.08 ± 0.08 (n = 17); Araujo, Ponzevera, et al., 2019); O19: Paleovase from the Loire estuary (France) (0.03 ± 0.03 (n = 12); Araujo, Ponzevera, et al., 2019); O20: Marine sediments from Beaufort sea (MESS-3 reference material) (0.01; K. Sullivan et al., 2020); O21: Marine sediments from British Columbia (Canada) (PACS Certified Reference Material) (0.03; K. Sullivan et al., 2020); O22: Modern marine sediments (Cariaco basin) (0.14 ± 0.08 (n = 2); Little, Vance, McManus, et al., 2017); O23: Modern marine sediments (California borderland basin) (0.14 ± 0.08 (n = 4); Little, Vance, McManus, et al., 2017); O24: Modern marine sediments (Black Sea) (0.2 ± 0.01 (n = 4); Little, Vance, McManus, et al., 2017); O25: Modern marine sediments (Peru margin) (0.32 (n = 1); Little, Vance, McManus, et al., 2017); O26: Modern marine sediments (Mexican margin) (0.16 ± 0.03 (n = 3); Little, Vance, McManus, et al., 2017); O27: North Atlantic marine sediment (HISS-1 Certified Reference Material) (0.05 ± 0.02; Takano, Liao, Tian, et al., 2020); O28: South Central Indian Ocean (<100 m) (0.5 ± 0.01 (n = 4); Takano, Tanimizu, et al., 2014); O29: South Central Indian Ocean (>300 m) (0.64 ± 0.03 (n = 12); Takano, Tanimizu, et al., 2014); O30: South Central Indian Ocean (1.1 ± 0.16 (n = 12); Vance, Archer, et al., 2008); O31: Western North Pacific Ocean (<100 m) (0.47 ± 0.03 (n = 6); Takano, Tanimizu, et al., 2014);

Figure 4. (**cont**.) O32: Western North Pacific Ocean (>300 m) (0.65 ± 0.04 (n = 12); Takano, Tanimizu, et al., 2014); O33: Eastern North Pacific Ocean (<100 m) (0.49 ± 0.06 (n = 7); Takano, Tanimizu, et al., 2014); O34: Eastern North Pacific Ocean (>300 m) (0.73 ± 0.06 (n = 18); Takano, Tanimizu, et al., 2014); O35: North East Pacific Ocean (1.14 ± 0.12 (n = 11); Vance, Archer, et al., 2008); O36: North East Pacific (0.85–1.35 (range); Bermin et al., 2006); O37: North Tasman sea (SW Pacific Ocean) (0.61 ± 0.16 (n = 15); Thompson and Ellwood, 2014); O38: Mid Tasman sea (SW Pacific Ocean) (0.7 ± 0.2 (n = 17); Thompson and Ellwood, 2014); O39: South Tasman sea (SW Pacific Ocean) (0.78 ± 0.17 (n = 16); Thompson and Ellwood, 2014); O40: Particles from Tasman sea (SW Pacific Ocean) (0.17 ± 0.15 (n = 7); Thompson and Ellwood, 2014); O41: Surface water (<200 m) from Kuroshio current along the East China Sea (0.47 ± 0.05 (n = 37); Takano, Liao, Ho, et al., 2022); O42: Deep water (>600 m) from Kuroshio current along the East China Sea (0.68 ± 0.02 (n = 17); Takano, Liao, Ho, et al., 2022); O43: Northern South China Sea (<400 m) (0.47 (n = 1); Takano, Liao, Tian, et al., 2020); O44: Northern South China Sea (>400 m) (0.68 ± 0.03 (n = 4); Takano, Liao, Tian, et al., 2020); 045: Particles from Northern South China Sea (0.13–0.36; Takano, Liao, Tian, et al., 2020); O46: Fe–Mn nodules from Pacific Ocean (0.54 ± 0.04 (n = 8); Little, Vance, Walker-Brown, et al., 2014); O47: Fe–Mn nodules from Indian Ocean (0.28 ± 0.39 (n = 8); Little, Vance, Walker-Brown, et al., 2014); O48: Fe–Mn nodules from Atlantic Ocean (0.33 ± 0.07 (n = 8); Little, Vance, Walker-Brown, et al., 2014); O49: Natural background sediment from Sepetiba Bay (Brazil) (0.2 (n = 1); Jeong, Araujo, Garnier, et al., 2023); O50: Sediment from Sepetiba bay (Brazil), impacted by smelter (0.32 ± 0.18 (n = 13); Jeong, Araujo, Garnier, et al., 2023); O51: Sediment from Northern Sepetiba bay (Brazil) (0.23 ± 0.1 (n = 12); Jeong, Araujo, Garnier, et al., 2023); O52: Metallurgic slag from Sepetiba bay (Brazil) (0.4 ± 0.2; Jeong, Araujo, Garnier, et al., 2023); O53: Sediments from Busan Harbor (South Korea) (0.27 ± 0.04 (n =7); Jeong, Araujo, Knoery, et al., 2023); O54: Domestic Antifoulings paints (South Korea) (0.48 ± 0.06 (n = 5); Jeong, Araujo, Knoery, et al., 2023); O55: Imported antifouling sources paints (South Korea) (0.39 ± 0.16 (n = 4); Jeong, Araujo, Knoery, et al., 2023); O56: Cu-contaminated Mediterranean sediments from marina of Port Camargue (France) (0.07 ± 0.12 (n = 25); Briant et al., 2022); O57: Antifouling paints Cu-contaminated Mediterranean marina of Port Camargue (0.54 ± 0.05 (n = 3); Briant et al., 2022).

Beyond these uncertainties on flux or isotopic signatures, work must be continued on particle dissolution processes (e.g., Little, Archer, et al., 2018; Thompson and Ellwood, 2014) as well as on processes occurring in estuarine zones. There is no data on these environments.

6. Conclusion

The objective of this work was to make an inventory of copper isotope signatures in the main reservoirs (rock, soil, river, oceans). What amplitudes, what signs? After almost 25 years of work carried out with precise measurements of these isotopic ratios, it is important to consider whether they can provide us useful constraints in the understanding of the cycle of large-scale elements. Some results can be confirmed while others today have too many uncertainties: (1) the isotopic signature of rocks shows a low amplitude; (2) the regions with sulfides or affected by acid mine drainage are those that exhibit the most important fractionations either for solids (rocks, precipitates, sediments) or for waters; (3) soils not impacted by human activities (industry, mine, winegrowing) have low variability; (4) Cu leached from the soils is heavier than the residual soil; (5) the global isotopic signature used today for the dissolved phase of rivers should, to my opinion, be improved by considering seasonal sampling and unsampled large river systems; (6) the particulate matter of rivers is more negative than the dissolved phase; (7) coastal mining areas are potentially a major source of copper to the global Ocean and can impact the isotopic signature of the global Ocean; (8) the dissolved phase of the Oceans is much heavier than the particulate phase; (9) the work of modelling Cu isotopic signatures in the World Ocean remains hazardous due to the uncertainty of the isotopic signature of river and atmospheric flows.

Declaration of interests

The authors do not work for, advise, own shares in, or receive funds from any organization that could benefit from this article, and have declared no affiliations other than their research organizations.

Acknowledgement

I would like to deeply thank you Nolwenn Lemaitre for helpful discussion.

References

Araujo, D. F., J. Knoery, N. Briant, et al., "Cu and Zn stable isotopes in suspended particulate matter sub-fractions from the northern Bay of Biscay help identify biogenic and geogenic particle pools", *Cont. Shelf. Res.* **244** (2022), article no. 104791.

Araujo, D. F., E. Ponzevera, N. Briant, J. Knoery, T. Sireau, M. Mojtahid, E. Metzger and C. Brach-Papa, "Assessment of the metal contamination evolution in the Loire estuary using Cu and Zn stable isotopes and geochemical data in sediments", *Marine Pollut. Bull.* **143** (2019), pp. 12–23.

Asael, D., A. Matthews, M.-B. Bar-Matthews and L. Halicz, "Copper isotope fractionation in sedimentary copper mineralization (Timna valley, Israel)", *Chem. Geol.* **243** (2007), pp. 238–254.

Babcsanyi, I., F. Chabaux, M. Granet, F. Meite, S. Payraudeau, J. Duplay and G. Imfeld, "Copper in soil fractions and runoff in a vineyard catchment: insights from copper stable isotopes", *Sci. Total Environ.* **557–558** (2016), pp. 154–162.

Baconnais, I., O. Rouxel, G. Dulaquais and M. Boye, "Determination of the copper isotope composition of seawater revisited: a case study from the Mediterranean Sea", *Chem. Geol.* **511** (2019), pp. 465–480.

Balistrieri, L. S., D. M. Borrok, R. B. Wanty and W. I. Ridley, "Fractionation of Cu and Zn isotopes during adsorption onto amorphous Fe(III) oxyhydroxide: experimental mixing of acid rock drainage and ambient river water", *Geochim. Cosmochim. Acta* **72** (2008), no. 2, pp. 311–328.

Barreira, J., D. F. Araujo, B. Q. A. Rodrigues, et al., "Copper isotopes as a tool to trace contamination in mangroves from an urbanized watershed", *Environ. Pollut.* **340** (2024), article no. 122785.

Bermin, J., D. Vance, C. Archer and P. J. Statham, "The determination of the isotopic composition of Cu and Zn in seawater", *Chem. Geol.* **226** (2006), pp. 280–297.

Bigalke, M., S. Weyer, J. Kobza and W. Wilcke, "Stable Cu and Zn isotope ratios as tracers of sources and transport of Cu and Zn in contaminated soil", *Geochim. Cosmochim. Acta* **74** (2010), pp. 6801–6813.

Bigalke, M., S. Weyer and W. Wilcke, "Copper isotope fractionation during complexation with insolubilized humic acid", *Environ. Sci. Technol.* **44** (2010), no. 14, pp. 5496–5502.

Bigalke, M., S. Weyer and W. Wilcke, "Stable Cu istope fractionation in soils during oxic weathering and podzolization", *Geochim. Cosmochim. Acta* **75** (2011), pp. 3119–3134.

Blotevogel, S., P. Oliva, S. Sobanska, et al., "The fate of Cu pesticides in vineyard soils: a case study using δ^{65}Cu isotope ratios and EPR analysis", *Chem. Geol.* **477** (2018), pp. 35–46.

Blotevogel, S., E. Schreck, S. Audry, et al., "Contribution of elemental contents and Cu and Sr isotope ratios to the understanding of pedogenetic processes and mechanisms involved in the soil-to-grape transfer (Soave vineyard, Italy)", *Geoderma* **343** (2019), pp. 72–85.

Borrok, D. M., D. A. Nimick, R. B. Wanty and W. I. Ridley, "Isotopic variations of dissolved copper and zinc in stream waters affected by historical mining", *Geochim. Cosmochim. Acta* **72** (2008), no. 2, pp. 329–344.

Boyle, E. A., F. R. Sclater and J. M. Edmond, "The distribution of dissolved copper in the Pacific", *Earth Planet. Sci. Lett.* **37** (1977), no. 1, pp. 38–54.

Brewer, G. J., "Copper toxicity in the general population", *Clin. Neurophysiol.* **121** (2010), no. 4, pp. 459–460.

Briant, N., R. Freydier, D. F. Araujo, S. Delpoux and F. Elbaz-Poulichet, "Cu isotope records of Cu-based antifouling paints in sediment core profiles from the largest European Marina, The Port Camargue", *Sci. Total Environ.* **849** (2022), article no. 157885.

Buu-Sao, D., "Faire advenir la « mine durable » en Europe ? Discours institutionnels et impératif de relance minière, de l'Union européenne à l'Andalousie", *Governance Rev.* **18** (2021), no. 2, pp. 16–41.

Chapman, J. B., T. F. D. Mason, D. J. Weiss, B. J. Coles and J. J. Wilkinson, "Chemical separation and isotopic variations of Cu and Zn from five geological reference materials", *Geostand. Geoanal. Res.* **30** (2005), pp. 5–16.

Chi-Fru, E., N. Perez-Rodriguez, C. A. Partin, et al., "Cu isotopes in marine black shales record the Great Oxidation Event", *Proc. Natl. Acad. Sci. USA* **113** (2016), no. 18, pp. 4941–4946.

Coutaud, M., M. Meheut, P. Glatzel, G. S. Pokrovski, J. Viers, J.-L. Rols and O. S. Pokrovsky, "Small changes in Cu redox state and speciation generate large isotope fractionation during adsorption and incorporation of Cu by a phototrophic biofilm", *Geochim. Cosmochim. Acta* **220** (2018), pp. 1–18.

Dong, S., R. Ochoa Gonzalez, R. M. Harrison, D. Green, R. North, D. Fowler and D. Weiss, "Isotopic signatures suggest an important contributions from recycled gasoline, road dust and non-exhaust traffic sources for copper, zinc, and lead in PM10 in London, United Kingdom", *Atmos. Environ.* **165** (2017), pp. 88–98.

Dong, S., D. J. Weiss, S. Strekopytov, K. Kreissig, Y. Sun, A. R. Baker and P. Formenti, "Stable isotope ratio measurements of Cu and Zn in mineral dust (bulk and size fractions) from the Taklimakan desert and the Sahel and in aerosols from the eastern tropical North Atlantic Ocean", *Talanta* **114** (2013), pp. 103–109.

Dótor-Almazán, A., M. A. Armienta-Hernández, O. Talavera-Mendoza and J. Ruiz, "Geochemical behavior of Cu and sulfur isotopes in the tropical mining region of Taxco, Guerrero (southern Mexico)", *Chem. Geol.* **471** (2017), pp. 1–12.

Ehrlich, S., I. Butler, L. Halicz, D. Rickard, A. Oldroyd and A. Matthews, "Experimental study of the copper isotope fractionation between aqueous Cu(II) and covellite (CuS)", *Chem. Geol.* **209** (2004), pp. 259–269.

El Azzi, D., J. Viers, M. Guiresse, A. Probst, D. Aubert, J. Caparros, K. Guizien and J.-L. Probst, "Origin and fate of copper in a small Mediterranean vineyard catchment: new insights from combined chemical extraction and δ^{65}Cu isotopic composition", *Sci. Total Environ.* **463–464** (2013), pp. 91–101.

Fekiacova, Z., S. Cornu and S. Pichat, "Tracing contamination sources in soils with Cu and Zn isotopic ratios", *Sci. Total Environ.* **517** (2015), pp. 96–105.

Fernandez, A. and D. M. Borrok, "Fractionation of Cu, Fe, and Zn isotopes during the oxidative weathering of sulfide-rich rocks", *Chem. Geol.* **264** (2009), no. 1–4, pp. 1–12.

Flemming, C. A. and J. T. Trevors, "Copper toxicity and chemistry in the environment: a review", *Water Air Soil Pollut.* **44** (1989), pp. 143–158.

Gaillardet, J., J. Viers and B. Dupré, "Trace element in river waters", in *Treatise on Geochemistry*, 2nd edition (Holland, H. D. and K. K. Turekian, eds.), Elsevier: Oxford, 2014, pp. 195–235.

Gelly, R., Z. Fekiacova, A. Guihou, E. Doelsch, P. Deschamps and C. Keller, "Lead, zinc, and copper redistributions in soils along a deposition gradient from emissions of a Pb–Ag smelter decommissioned 100 years ago", *Sci. Total Environ.* **665** (2019), pp. 502–512.

Guinoiseau, D., A. Gélabert, T. Allard, P. Louvat, P. Moreira-Turcq and M. F. Benedetti, "Zinc and copper behaviour at the soil–river interface: new insights by Zn and Cu isotopes in the organic-rich Rio Negro basin", *Geochim. Cosmochim. Acta* **213** (2017), pp. 178–197.

Ilina, S. M., J. Viers, S. A. Lapitsky, et al., "Stable (Cu, Mg) and radiogenic (Sr, Nd) isotope fractionation in colloids of boreal organic-rich waters", *Chem. Geol.* **342** (2013), pp. 63–75.

Jeong, H., D. F. Araujo, J. Garnier, D. Mulholland, W. Machado, B. Cunha and E. Ponzevera, "Copper and lead isotope records from and electroplating activity in sediments and biota from Sepetiba Bay (souteastern Brasil)", *Mar. Pollut. Bull.* **190** (2023), article no. 114848.

Jeong, H., D. F. Araujo, J. Knoery, N. Briant and K. Ra, "Isotopic (Cu, Zn, and Pb) and elemental fingerprints of antifouling paints and their potential use for environmental forensic investigations", *Environ. Pollut.* **322** (2023), article no. 121176.

Johnson, C. M., B. L. Beard and F. Albarede, "Geochemistry of non-traditional stable isotopes", *Rev. Mineral. Geochem.* **55** (2004), pp. 1–22.

Junqueira, T. P., D. F. Araujo, A. L. Harrison, K. Sullivan, M. I. Leybourne and B. Vriens, "Contrasting copper concentrations and isotopic compositions in two Great Makes watersheds", *Sci. Total Environ.* **904** (2023), article no. 166360.

Kim, D.-M., H.-L. Kwon and D.-G. Im, "Determination of contamination sources and geochemical behaviors of metals in soil of a mine area using Cu, Pb, Zn and S isotopes and positive matrix factorization", *J. Hazard Mater.* **447** (2023), article no. 130827.

Kimball, B. E., R. Mathur, A. C. Dohnalkova, A. J. Wall, R. L. Runkel and S. L. Brantley, "Copper isotope fractionation in acid mine drainage", *Geochim. Cosmochim. Acta* **73** (2009), pp. 1247–1263.

Komárek, M., G. Ratié, Z. Vaňková, A. Šípková and V. Chrastný, "Metal isotope complexation with environmentally relevant surfaces: opening the isotope fractionation black box", *Crit. Rev. Environ. Sci. Technol.* **52** (2021), no. 20, pp. 3573–3603.

Kribek, B., A. Sipkova, V. Ettler, et al., "Variability of the copper isotopic composition in soil and grass affected by mining and smeting in Tsunemb, Namibia", *Chem. Geol.* **493** (2018), pp. 121–135.

Kusonwiriyawong, C., M. Bigalke, F. Abgottspon, M. Lazarov and W. Wilcke, "Response of Cu partitioning to flooding: a δ^{65}Cu approach in a carbonatic alluvial soil", *Chem. Geol.* **420** (2016), pp. 69–76.

Kusonwiriyawong, C., M. Bigalke, S. Cornu, D. Montagne, Z. Fekiacova, M. Lazaroc and W. Wilcke, "Response of copper concentrations and stable isotope ratios to artificial drainage in a French Retisol", *Geoderma* **300** (2017), pp. 44–54.

Larson, P. B., K. Maher, F. C. Ramos, Z. Chang, M. Gaspar and L. D. Meinert, "Copper isotope ratios in magmatic and hydrothermal ore-forming environments", *Chem. Geol.* **201** (2003), pp. 337–350.

Li, L., J. Ni, F. Chang, et al., "Global trends in water and sediment fluxes of the world's large rivers", *Sci. Bull.* **65** (2020), no. 1, pp. 62–69.

Li, W., S. E. Jackson, N. J. Pearson, O. Alard and W. Chappell, "The Cu isotopic signature of granites from the Lachlan Fold Belt, SE Australia", *Chem. Geol.* **258** (2009), pp. 38–49.

Li, Z. Q., Z. M. Yang, X. K. Zhu, Z. Q. Hou, S. Z. Li, Z. H. Li and Y. Wang, "Cu isotope composition of Qulong porphyry Cu deposit, Tibet", *Acta Geol. Sin.* **83** (2009), pp. 1985–1996.

Little, S. H., C. Archer, A. Milne, C. Schlosser, E. P. Achterberg, M. C. Lohan and D. Vance, "Paired dissolved and particulate phase Cu isotope distributions in the South Atlantic", *Chem. Geol.* **502** (2018), pp. 29–43.

Little, S. H., S. Munson, J. Prytulak, B. J. Coles, S. J. Hammond and M. Widdowson, "Cu and Zn isotope fractionation during extreme chemical weathering", *Geochim. Cosmochim. Acta* **263** (2019), pp. 85–107.

Little, S. H., D. Vance, J. McManus, S. Severmann and T. W. Lyons, "Copper isotope signatures in modern marine sediments", *Geochim. Cosmochim. Acta* **212** (2017), pp. 253–273.

Little, S. H., D. Vance, C. Walker-Brown and W. M. Landing, "The oceanic mass balance of copper and zinc isotopes, investigated by analysis of their inputs, and outputs to ferromanganese oxide sediments", *Geochim. Cosmochim. Acta* **125** (2014), pp. 673–693.

Liu, J.-H., J. Cheng, L. Zhou, L.-P. Feng, Y.-T. Hu and T. J. Algeo, "Copper and gallium isotopic behavior in highly weathered soils", *Chem. Geol.* **594** (2022), article no. 120757.

Liu, S.-A., J. Huang, J. Liu, et al., "Copper isotopic composition of the silicate Earth", *Earth Planet. Sci. Lett.* **427** (2015), pp. 95–103.

Liu, S.-A., F.-Z. Teng, S. Li, G.-J. Wei, J.-L. Ma and D. Li, "Copper and iron isotope fractionation during weathering and pedogenesis: insights from saprolite profiles", *Geochim. Cosmochim. Acta* **146** (2014), pp. 59–75.

Lottermoser, B. G., P. M. Ashley and D. C. Lawie, "Environmental geochemistry of the Gulf Creek copper mine area, northeastern New South Wales, Australia", *Environ. Geol.* **39** (1999), pp. 61–74.

Lv, Y., S.-A. Liu, J.-M. Zhu and S. Li, "Copper and zinc isotope fractionation during deposition and weathering of highly metalliferous black shales in central china", *Chem. Geol.* **445** (2016), pp. 24–35.

Machu, Y., D. Aubert, W. Ludwig, B. Charrière, J. Sola, C. Sotin and M. Henry, "Global budget assessment of natural and anthropogenic particulate copper fluxes to the Gulf of Lions", *Sci. Total. Environ.* **956** (2024), article no. 177266.

Mahan, B., R. Mathur, I. Sanislav, P. Rea and P. Dirks, "Cu isotopes in groundwater for hydrogeochemical mineral exploration: a case study using the world-class Mount Isa Cu–Pb–Zn deposit (Australia)", *Appl. Geochem.* **148** (2023), article no. 105519.

Maréchal, C. N., P. Télouk and F. Albarede, "Precise analysis of copper and zinc isotopic compositions by plasma-source mass spectrometry", *Chem. Geol.* **156** (1999), pp. 251–273.

Markl, G., Y. Lahaye and G. Schwinn, "Copper isotopes as monitors of redox processes in hydrothermal mineralization", *Geochim. Cosmochim. Acta* **70** (2006), pp. 4215–4228.

Masbou, J., J. Viers, J. A. Grande, et al., "Strong temporal and spatial variation of dissolved Cu isotope composition in acid mine drainage under contrasted hydrological conditions", *Environ. Pollut.* **266** (2020), article no. 115104.

Mathur, R., L. Jin, V. Prush, J. Paul, C. Ebersole, A. Fornadel, J. Z. Williams and S. Brantley, "Cu isotopes and concentrations during weathering of black shale of the Marcellus Formation, Huntingdon County, Pennsylvania (USA)", *Chem. Geol.* **304–305** (2012), pp. 175–184.

Mathur, R., L. A. Munk, B. Townley, et al., "Tracing low-temperature aqueous metal migration in mineralized watersheds with Cu isotope fractionation", *Appl. Geochem.* **51** (2014), pp. 109–115.

Mathur, R., J. Ruiz, M. J. Casselman, P. Megaw and R. van Egmond, "Use of Cu isotopes to distinguish primary and secondary Cu mineralization in the Cañariaco Norte porphyry copper deposit, Northern Peru", *Miner. Deposita* **47** (2012), pp. 755–762.

Mathur, R., J. Ruiz, S. Titley, L. Liermann, H. Buss and S. Brantley, "Cu isotopic fractionation in the supergene environment with and without bacteria", *Geochim. Cosmochim. Acta* **69** (2005), no. 22, pp. 5233–5246.

Mathur, R., S. Titley, F. Barra, et al., "Exploration potential of Cu isotope fractionation in porphyry copper deposits", *J. Geochem. Explor.* **102** (2009), pp. 1–6.

Mihaljevic, M., A. Jarosikova, V. Ettler, et al., "Copper isotopic record in soils and tree rings near a copper smelter, Copperbelt, Zambia", *Sci. Total Environ.* **621** (2018), pp. 9–17.

Mirnejad, H., R. Mathur, M. Einali, M. Dendas and S. Alirezaei, "A comparative copper isotope study of porphyry copper deposits in Iran", *Geochem. Explor. Environ. Anal.* **10** (2010), pp. 413–418.

Moynier, F., D. Vance, T. Fujii and P. Savage, "The isotope geochemistry of zinc and copper", *Rev. Mineral. Geochem.* **82** (2017), no. 1, pp. 543–600.

Navarrete, J. U., D. M. Borrok, M. Viveros and J. T. Ellzey, "Copper isotope fractionation during surface adsorption and intracellular incorporation by bacteria", *Geochim. Cosmochim. Acta* **75** (2011), pp. 784–799.

Nie, L. M., Z. Q. Li and X. J. Fang, "Cu isotope fractionation during magma evolution process of Qulong porphyry copper deposit", *Tibet Mineral Depos.* **31** (2012), no. 4, pp. 718–726.

Nieto, J. M., A. M. Sarmiento, M. Olias, C. R. Canovas, I. Riba, J. Kalman and T. A. Delvalls, "Acid mine drainage pollution in the Tinto and Odiel rivers (Iberian Pyrite Belt, SW Spain) and bioavailability of the transported metals to the Huelva Estuary", *Environ. Int.* **33** (2007), no. 4, pp. 445–455.

Novak, M., A. Sipkova, V. Chrastny, et al., "Cu–Zn isotope constraints on the provenance of air pollution in central Europe: using soluble and insoluble particles in snow and rime", *Environ. Pollut.* **218** (2016), pp. 1135–1146.

Ochoa Gonzalez, R., S. Strekopytov, F. Amato, X. Querol, C. Reche and D. Weiss, "New insights from zinc and copper isotopic composition into the sources of atmospheric particulate matter from two major European cities", *Environ. Sci. Technol.* **50** (2016), pp. 9816–9824.

Olias, M., C. R. Canovas, J.-M. Nieto and A. M. Sarmiento, "Evaluation of the dissolved contaminant load transported by the Tinto and Odiel rivers (south west Spain)", *Appl. Geochem.* **21** (2006), no. 10, pp. 1733–1749.

Packman, H., S. H. Little, A. R. Baker, et al., "Tracing natural and anthropogenic sources of aerosols to the Atlantic Ocean using Zn and Cu isotopes", *Chem. Geol.* **610** (2022), article no. 121091.

Perez Rodriguez, N., E. Engström, I. Rodushkin, P. Nason, L. Alakangas and B. Öhlander, "Copper and iron isotope fractionation in mine tailings at the Laver and Kristineberg mines, northern Sweden", *Appl. Geochem.* **32** (2013), pp. 204–215.

Petit, J. C. J., J. de Jong, L. Chou and N. Mattielli, "Development of Cu and Zn isotope MC-ICP-MS measurements: application to suspended particulate matter and sediments from the Scheldt estuary", *Geostand. Geoanal. Res.* **32** (2008), no. 2, pp. 149–166.

Petit, J. C. J., J. Schäfer, A. Coynel, et al., "Anthropogenic sources and biogeochemical reactivity of particulate and dissolved Cu isotopes in the turbidity gradient of the Garonne River (France)", *Chem. Geol.* **359** (2013), pp. 125–135.

Pokrovsky, O., J. Viers, E. E. Emnova, E. I. Kompantseva and R. Freydier, "Copper isotope fractionation during its interaction with soil and aquatic microorganisms and metal oxy(hydr)oxides: possible structural control", *Geochim. Cosmochim. Acta* **72** (2008), pp. 1742–1757.

Ren, M., L. Zheng, D. Wang, X. Chen, X. Dong, X. Wei and H. Cheng, "Copper isotope ratios allowed for quantifying the contribution of coal mining and combustion to total soil copper concentrations in China", *Environ. Pollut.* **308** (2022), article no. 119613.

Ryan, B. M., J. K. Kirby, F. Degryse, K. Scheiderich and M. J. McLaughlin, "Copper isotope fractionation during equilibration with natural synthetic ligands", *Environ. Sci. Technol.* **48** (2014), no. 15, pp. 8620–8626.

Sarjoughian, F., F. Shubin, S. Asadi, F. Moore and M. Haschke, "Cu isotope patterns of whole rocks in the Kerman porphyry copper belt, southeastern Urumieh Dokhtar magmatic arc, Iran", *J. Geochem. Explor.* **256** (2024), article no. 107329.

Savage, P. S., F. Moynier, H. Chen, J. Shofner, J. Siebert, J. Badro and I. S. Puchtel, "Copper isotope evidence for large-scale sulphide fractionation during Earth's differentiation", *Geochem. Perspect. Lett.* **1** (2015), pp. 53–64.

Sherman, D. M. and S. H. Little, "Isotopic disequilibrium of Cu in marine ferromanganese crusts: evidence from ab initio predictions of Cu isotope fractionation on sorption to birnessite", *Earth Planet. Sci. Lett.* **549** (2020), article no. 116540.

Song, S., R. Mathur, J. Ruiz, D. Chen, N. Allin, K. Guo and W. Kang, "Fingerprinting two metal contaminants in streams with Cu isotopes near the Dexing Mine, China", *Sci. Total Environ.* **544** (2016), pp. 677–685.

Sossi, P. A., G. P. Halverson, O. Nebel and S. M. Eggins, "Combined separation of Cu, Fe and Zn from rock matrices and improved analytical protocols for stable isotope determination", *Geostand. Geoanal. Res.* **39** (2014), pp. 129–149.

Souto-Oliveira, C. E., M. Babinski, D. F. Araujo and M. F. Andrade, "Multi-isotopic fingerprints (Pb, Zn, Cu) applied for urban aerosol source apportionment and discrimination", *Sci. Total Environ.* **626** (2018), pp. 1350–1366.

Sullivan, K., D. Layton-Matthews, M. Leybourne, J. Kidder, Z. Mester and L. Yanh, "Copper isotopic, analysis in geological and biological reference materials by MC-ICP-MS", *Geostand. Geoanal. Res.* **44** (2020), pp. 349–362.

Sullivan, K. V., J. A. Kidder, T. P. Junqueira, F. Vanhaecke and M. L. Leybourne, "Emerging applications of high-precision Cu isotopic analysis by MC-ICP-MS", *Sci. Total Environ.* **838** (2022), article no. 156084.

Takano, S., W.-H. Liao, T.-Y. Ho and Y. Sohrin, "Isotopic evolution of dissolved Ni, Cu and Zn along the Kuroshio through the east China", *Sea Mar. Chem.* **243** (2022), article no. 104135.

Takano, S., W.-H. Liao, H.-A. Tian, K.-F. Huang, T.-Y. Ho and Y. Sohrin, "Sources of particulate Ni and Cu in the water column of the northern South China Sea: evidence from elemental and isotope ratio sin aerosols and sinking particles", *Mar. Chem.* **219** (2020), article no. 103751.

Takano, S., M. Tanimizu, T. Hirata and Y. Sohrin, "Isotopic constraints on biogeochemical cycling of copper in the ocean", *Nat. Commun.* **5** (2014), article no. 5663.

Takano, S., M. Tsuchiya, S. Imai, Y. Yamamoto, Y. Fukami, K. Suzuki and Y. Sohrin, "Isotopic analysis of nickel, copper, and zinc in various freshwater samples for source identification", *Geochem. J.* **55** (2021), pp. 171–183.

Teng, F.-Z., N. Dauphas and J. M. Watkins, "Non-traditional stable isotopes: retrospective and prospective", *Rev. Mineral. Geochem.* **82** (2017), no. 1, pp. 1–26.

Thapalia, A., D. M. Borrok, P. C. Van Metre, M. Musgrove and E. R. Landa, "Zn and Cu isotopes as tracers of anthropogenic contamination in a sediment core from an urban lake", *Environ. Sci. Technol.* **44** (2010), pp. 1544–1550.

Thompson, C. M. and M. J. Ellwood, "Dissolved copper isotope biogeochemistry in the Tasman Sea, SW Pacific Ocean", *Mar. Chem.* **165** (2014), pp. 1–9.

Tu, Y.-J., P.-C. Luo, Y.-L. Li, J. Liu, T.-T. Sun, G.-J. Li and Y.-P. Duan, "Seasonal heavy metal speciation in sediment and source tracking via Cu isotopic composition in Huangpu River, Shanghai, China", *Ecotoxicol. Environ. Saf.* **260** (2023), article no. 115068.

Vance, D., C. Archer, J. Bermin, J. Perkins, P. J. Statham, M. C. Lohan, M. J. Ellwood and R. A. Mills, "The copper isotope geochemistry of rivers and the oceans", *Earth Planet. Sci. Lett.* **274** (2008), pp. 204–213.

Vance, D., L. Matthews, A. Keech, C. Archer, G. Hudson, J. Pett-Ridge and O. A. Chadwick, "The behaviour of Cu and Zn isotopes during soil development: controls on the dissolved load of rivers", *Chem. Geol.* **445** (2016), pp. 36–53.

Viers, J., B. Dupré and J. Gaillardet, "Chemical composition of world'rivers suspended sediments: new insights from a new database", *Sci. Total. Environ.* **407** (2009), pp. 853–868.

Viers, J., R. Freydier, J.-A. Grande, et al., "The use of copper isotopes for understanding metal transfer mechanisms within the continuum mine—river—dam (Huelva Region, Spain)", *Environ. Sci. Pollut. Res.* **30** (2023), no. 2, pp. 1–20.

Viers, J., J. A. Grande, C. Zouiten, et al., "Are Cu isotopes a useful tool to trace metal sources and processes in acid mine drainage (AMD) context?", *Chemosphere* **193** (2018), pp. 1071–1079.

Wang, P., G. Dong, M. Santosh, K. Liu and X. Li, "Copper isotopes trace the evolution of skarn ores: a case study from the Hongshan-Hongniu Cu deposit, southwest China", *Ore Geol. Rev.* **88** (2017), pp. 822–831.

Wang, Q., L. Zhou, S. H. Little, J. Liu, L. Feng and S. Tong, "The geochemical behaviour of Cu and its isotopes in the Yangtze River", *Sci. Total Environ.* **728** (2020), article no. 138428.

Wang, R.-R., H.-M. Yu, W.-H. Cheng, Y.-C. Liu, G.-L. Zhang, De-C. Li and F. Huang, "Copper migration and isotope fractionation in a typical paddy soil of the Yangtze Delta", *Sci. Total Environ.* **821** (2022), article no. 153201.

Wang, Z., J.-W. Park, X. Wang, Z. Zou, J. Kim, P. Zhang and M. Li, "Evoluytion of copper isotopes in arc systems: insights from lavas and molten sulfur in Niuatahi volcano, Tonga rear arc", *Geochim. Cosmochim. Acta* **250** (2019), pp. 18–33.

Wu, S., Y. Zheng, D. Wang, H. Chang and M. Tan, "Variation of copper isotopes in chalcopyrite from dabu porphyry Cu–Mo deposit in Tibet and implications for mineral exploration", *Ore Geol. Rev.* **90** (2017), pp. 14–24.

Xia, B., Y. Huang, X. Pei and C. Liu, "Application of Cu isotopes to identify Cu sources in soils impacted by multiple anthropogenic activities", *Sci. Total Environ.* **905** (2023), article no. 167114.

Zeng, J. and G. Han, "Preliminary copper isotope study on particulate matter in Zhujiang River, soutwest China: application for source identification", *Ecotoxicol. Environ. Saf.* **198** (2020), article no. 110663.

Zhao, Y., S.-A. Liu, C. Xue, R. Mathur, D. T. A. Symons and J. Ke, "Copper isotope fractionation in magmatic Ni–Cu mineralization systems associated with the variation of oxygen fugacity in silicate magmas", *Geochim. Cosmochim. Acta* **338** (2022), pp. 250–263.

Zheng, X., G. Han and B. Liang, "Distribution of Cu in agricultural soils with different land uses through stable analysis", *Ecol. Indic.* **143** (2023), article no. 109903.

Zheng, Y.-C., S.-A. Liu, C.-D. Wu, et al., "Cu isotopes reveal initial Cu enrichment in sources of giant porphyry deposits in a collisional setting", *Geology* **47** (2019), no. 2, pp. 135–138.